2014 IEEE International Conference on Robotics & Automation (ICRA)
Hong Kong Convention and Exhibition Center
May 31 - June 7, 2014. Hong Kong, China

Pitch and Yaw Control of a Robotic Insect using an Onboard Magnetometer

E. Farrell Helbling, Sawyer B. Fuller, and Robert J. Wood

***Abstract*— The Harvard RoboBee was the first fly-sized vehicle to lift its own weight. This vehicle has previously demonstrated controlled flight maneuvers, but this required an array of external cameras to precisely track its trajectory. Developing flight-worthy sensors to eliminate the need for external motion capture is an area of active study. In this paper, we consider an onboard analog magnetometer. We show that the sensor meets the size, weight, and power requirements for the RoboBee and can provide feedback on angular position for pitch and yaw angle control. We show that this sensor can provide an accurate angle reading despite proximity to the piezoelectric actuators of this vehicle. This is likely because the actuators are driven by electrostatic forces rather than the electromagnetic forces that drive the electric motors of larger aircraft. This sensor provided sufficient bandwidth to enable rapid pitch angle maneuvers within 200ms on a RoboBee constrained to rotate only about its pitch axis. We also show it operating in a feedback loop to control heading angle, the first demonstration of controlling yaw orientation at this scale.**

I. Introduction

The Harvard RoboBee (Fig. 1) presents many unique engineering design and control challenges because the low mass of the system (50–500mg) and centimeter-scale require careful consideration of size, weight, and power for each component. The RoboBee is the first flapping-wing micro-air vehicle (FWMAV) under one gram to demonstrate controlled flight under external power [1]. Previous work has demonstrated controlled takeoff, hovering, lateral maneuvers, and landing [2]; however, in these flights, external motion capture cameras (Vicon) were used to determine the position and orientation of the robot. In order to attain autonomous flight, sensors need to be integrated into the robot for both proprioception and exteroception.

Previous studies have focused on biomimetic sensor packages for FWMAV, [3] [4]. Recent work has demonstrated a number of these biomimetic sensors integrated on the RoboBee including optical flow [5], ocelli and antennae [6], with demonstrations of altitude and pitch control. Researchers have also determined that insects determine orientation with magnetoreception [7] and polarization [8]. This kind of feedback may prove beneficial for similarly-sized robots for navigation or flight stabilization. To determine the final combination of sensors that will be equipped on the RoboBee, each sensor needs to be characterized – analyzing the power requirements, weight, output rate, resolution, and noise sensitivity. In this work, we discuss the characterization of a commercial anisotropic magnetoresistive (AMR) sensor. We demonstrate that it is capable of providing feedback to control motions about pitch and yaw of a RoboBee while constrained on a wire.

The authors are with the School of Engineering and Applied Sciences, Harvard University, Cambridge MA 02138 USA and the Wyss Institute for Biologically Inspired Engineering, Harvard University, Boston MA 02115, USA ehelbling@seas.harvard.edu

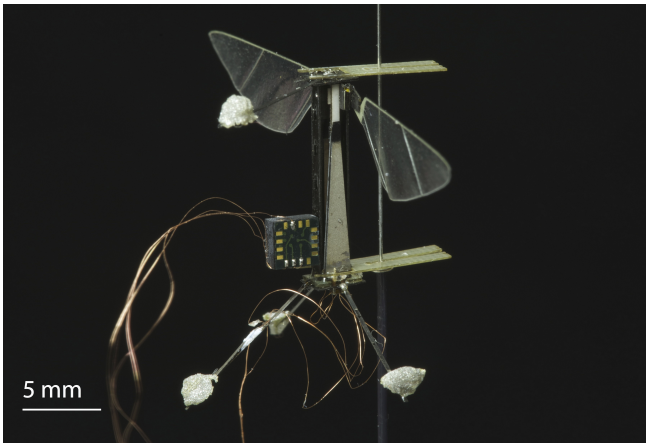

Fig. 1. Photo of the Harvard RoboBee attached to a wire to allow rotation about the yaw axis and prevent motion about pitch and roll. Clips are added to the top and bottom of the robot for attachment. The sensor is mounted to the anterior of the robot.

II. Magnetoresistive Sensors

The magnetoresistive effect was first discovered in ferromagnetic materials in the mid-19th century [9]. This material property allows the magnetic field to be measured by detecting changes in resistance. Sensors that utilize magnetoresistance for absolute angle control have become more common since the discovery of the giant magnetoresistive (GMR) effect [10] [11]. The large change in resistance (5–80%) [12] lends itself to more sensitive applications than AMR sensors which have a 2–5% resistance change [13]. Widely used by IBM as a low-field angle detector in the spin valve magnetic read heads of computer hard drives [14], these sensors have also proven useful in navigation [15] and current detection [16]. Magnetometers are not typically used in unmanned aerial vehicle (UAV) applications due to the local magnetic fields generated by onboard motors. The RoboBee, however, is driven by piezoelectric actuators, which have not been shown to generate magnetic fields because of their high voltages and low currents [17]. Though GMR sensors have a wide detection range, approximately 1– 10^8Ga [18], this detection range falls outside of the Earth's magnetic field range of 1–500mGa, so we consider AMR sensors in this work.

TABLE I

SPECIFICATIONS OF THE HMC1043

Characteristic	Typical Value
Area	3×3 mm
Height	1.4 mm
Mass	22 mg
Magnetic Field Range	± 6 Ga
Resolution	2 mGa, 0.4% of Earth's Field
Sensitivity	1 mV/V/Ga
Power	3 V, 5 mA
Bandwidth	5 MHz

A. AMR Sensor

In current uses of AMR technology, a thin permalloy (nickel-iron) film is deposited on silicon, which allows the sensors to be rapidly manufactured and used in integrated circuits [18]. The permalloy is cut into resistive strips and exposed to a high magnetic field to pre-align the magnetic fields of each resistor for high sensitivity. The resistors are then configured in a Wheatstone bridge to detect the direction and magnitude of a magnetic field along an axis.

In this work we characterize the Honeywell HMC1043 [19]. The dimensions, low mass, and moderate power consumption of the sensor are small enough for integration onto the RoboBee (Fig. 1) [20]. The detection range indicates that the sensor can accurately detect the magnitude and direction of the Earth's magnetic field. Finally the high bandwidth is sufficient to produce low latency orientation information (see Table I for a full list of specifications).

B. Interface

In the presence of an applied magnetic field, the change in resistance can be measured by taking the difference of the two outputs of the bridge circuit. With a sensitivity of 1 mV/V/Ga, in the presence of the Earth's magnetic field (approximately 1Ga) and with a supplied voltage of 3V, the signal from the magnetometer varies by approximately 3 mV/V/Ga. Using two ganged off board amplifiers (LMV344 and LM741) and standard passive components, this signal is amplified by 1,000 to provide a range of 3.3 – 7.3 V with a resolution of 1.5V/rad, compatible with the input voltage range of 0 – 10V of our data acquisition system.

III. PITCH CONTROL

We investigated the extent to which the signal was disrupted by the piezo actuators, the vibration induced by flapping wings and whether the noise level was low enough to function in a fast feedback loop.

A. Calibration

We attached the sensor to a rotating axle whose angle is measured by a potentiometer that is connected to the end of the axle as described in [6] (Fig. 2). As the device was rotated, the voltage signal from the sensor varied in proportion to the magnetic field strength along the z-component of the normal vector of the sensor according to:

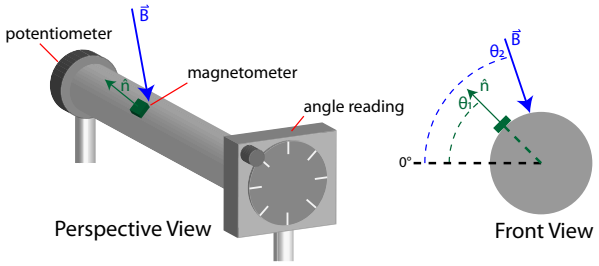

Fig. 2. (left): Calibrating the magnetometer. The magnetometer (green) was attached to a rotating axle whose angular position could be measured with a potentiometer. The angular position was recorded simultaneously with the signal from the magnetometer. The magnetic field vector is shown in blue, and is represented as an angle greater than the expected geomagnetic field vector due to the effect of nearby equipment. (right): A visualization of the planar projection of vectors and angles used in calibration.

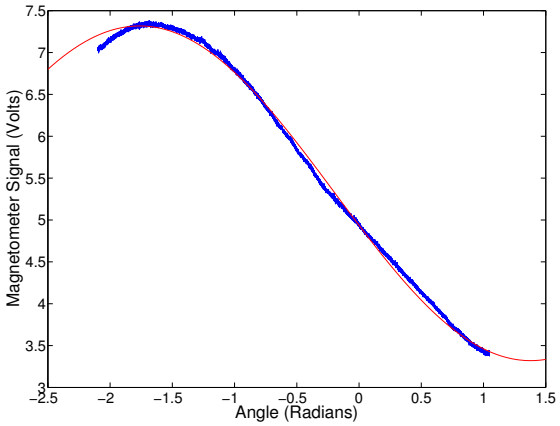

Fig. 3. Example calibration plot from the magnetometer. The measured angle in radians is along the x-axis and voltage signal from the sensor is along the y-axis. The raw signal from the magnetometer (blue) and the fitted curve (red) are plotted against the measured angle in radians.

$$\begin{aligned} V &= V_0 + k\overrightarrow{B}\cdot\hat{n} \\ &= V_0 + k|B|\cos(\theta_2 - \theta_1) \end{aligned} \tag{1}$$

where V_0 is the initial offset of the voltage signal from the magnetometer after amplification, k is a proportionality constant that incorporates the change in resistivity of the permalloy and subsequent amplification, $\overrightarrow{B}$ represents the magnetic field, $\hat{n}$ is the unit normal vector of the measured axis of the sensor, θ_2 is the angle from $\overrightarrow{B}$ to horizontal (inclination), and θ_1 is the measured elevation of the magnetometer (Fig. 2). In the above equation, both the magnitude and direction of the magnetic field are unknown. Using (1), we calibrated the sensor with three parameters, using the MATLAB 'fit' command and specifying the fit type as:

$$y = a\cos(x + b) + c \tag{2}$$

The sensor was rotated on the axle through 180°, from 60° to -120°, encompassing the expected operation range of about 90° (±45° tilt angle). Because both phase and

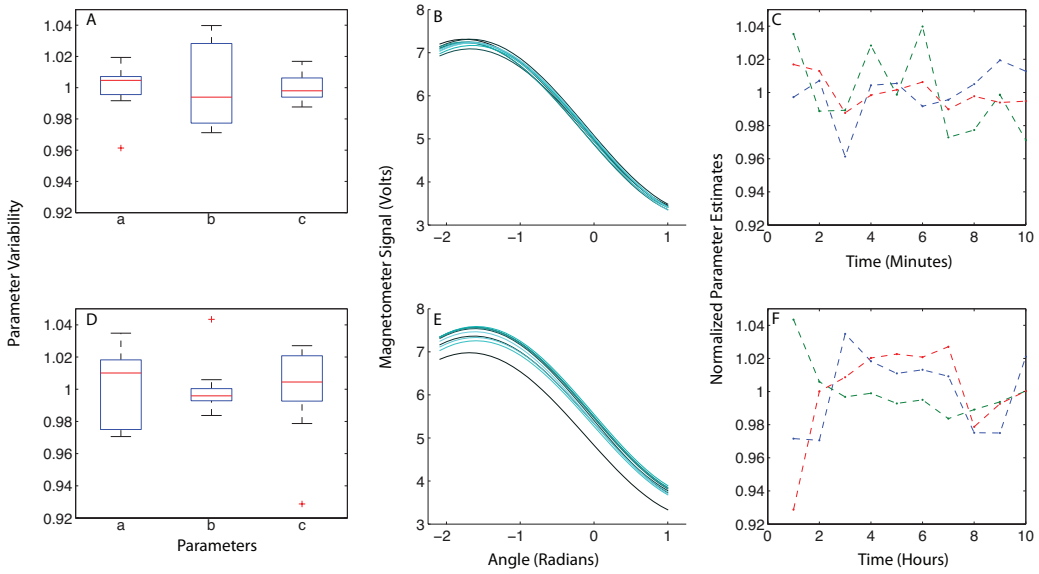

Fig. 4. A and D show the variability of parameters in the fit $y = a\cos(x + b) + c$ (median and 25^{th}–75^{th} percentiles) for ten tests, normalized by the mean. For clarity, the ten fits are plotted in B and E as a visualization of this spread. To visualize the drift in the parameter values, a (blue), b (green), c (red) are plotted with time. A, B and C display variability over ten minutes, while D, E, and F display variability over ten hours.

magnitude are unknown in the fit, the sensor had to be rotated through a larger range to capture one of the maximums of the sinusoidal fit. The magnetometer signal was plotted against the angles determined by the potentiometer and fit to the calibration constants. Fig. 3 demonstrates a typical fitting. The maximum of the sinusoidal fit was measured to be $-99°$, an inclination angle larger than that of the geomagnetic field (-67° at a latitude of 42° N). This indicates that the magnetometer is measuring an artificial field due to the local effects of nearby equipment.

In order to characterize the robustness of the sensor, calibration data were recorded over the course of a day. Fig. 4 displays two experiments with measured data over the course of ten minutes (Fig. 4A, 4B, & 4C) and ten hours (Fig. 4D, 4E, & 4F). We calibrated the sensor once a minute every ten minutes to determine how quickly the measured signal from the magnetometer would change in a relatively short period of time. As can be seen in Fig. 4A, 75% of the data for the amplitude (a) and the offset (c) fall within 1% of the mean. For the phase (b), which has a noticeably larger spread, 75% of the data falls within 4% of the mean. Using our fit parameters, the variability we measured suggests that the sensor can accurately determine the angle to within 2°. The parameters vary more noticeably over the course of ten hours (Fig. 4E). However, 75% of the data for each parameter is within 4% of the mean (Fig. 4D). As can be seen in Fig. 4C & 4F, there is no trend in the parameter estimates over time, indicating that the largest source of error is not the internal characteristics of the sensor, but rather external shifts in the applied magnetic field.

In addition to the presence of an unpredictable magnetic field signal, the largest source of deviation from the mean is due to the wire leading to the sensor. The sensor's signal is carried through thin copper wire to two off board amplifiers. This introduces noise into the system, and contact with the signal wires can cause large variations in measured signal at the last amplification stage. To minimize this effect, the amplifiers should be added onboard the robot to diminish some of the noise in the system.

Fig. 3 and Fig. 4 show a monotonic fit through a tilt angle of $\pm 60°$. With a signal range of approximately 3V and measured standard deviation of 12mV, as well as accuracy within 2°, the uncertainty in lateral position for a hovering RoboBee using this sensor and gains in [2] would be $\pm$4cm.

B. Absolute Angle Control

We attached the sensor to the underside of the robot (Fig. 5), which was then mounted on a wire that limited the motion to only the pitch axis (see Fig. 6 for axis convention). We applied a fixed amplitude and frequency to the wings of 300V and 90Hz, respectively. In order to generate a pitch torque, the mean stroke angle is varied by adjusting the mean voltage of the sinusoid that drives the wings [21]. We were able to design a feedback loop that would change the mean voltage of the sinusoid based on the measured angle of the magnetometer. Inside the feedback loop was a PD controller that was based on the estimated rotational moment of inertia of the robot [6]:

$$u(t) = K_P(\theta_m(t) - \theta_d(t)) + K_D\frac{d}{dt}(\theta_m(t) - \theta_d(t)) \quad (3)$$

where $u(t)$ is the commanded pitch torque, K_P is the proportional gain, θ_m is the measured angle from the magnetometer,

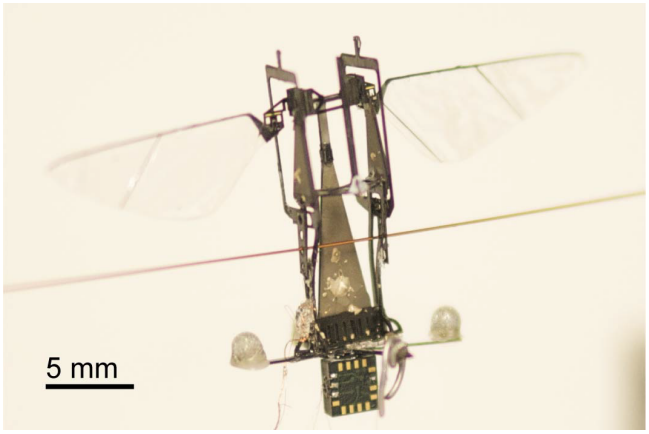

Fig. 5. Photo of a previous generation of the RoboBee on a wire. The generation displayed here and that in Fig. 1 are equivalent in pitch torque production; however the previous generation is more convenient for mounting a wire through the pitch axis. The wire prevented motion around the roll and yaw axes. The sensor is attached to the underside of the bee. A small amount of solder was added at the bottom to keep the bee in a neutral upright orientation.

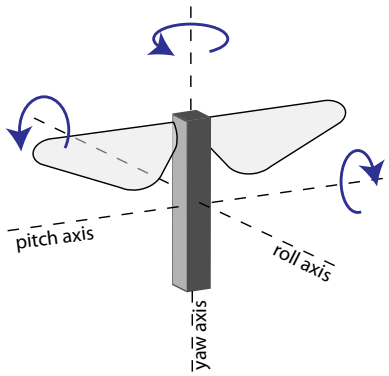

Fig. 6. Definition of the pitch, roll and yaw axes of the RoboBee.

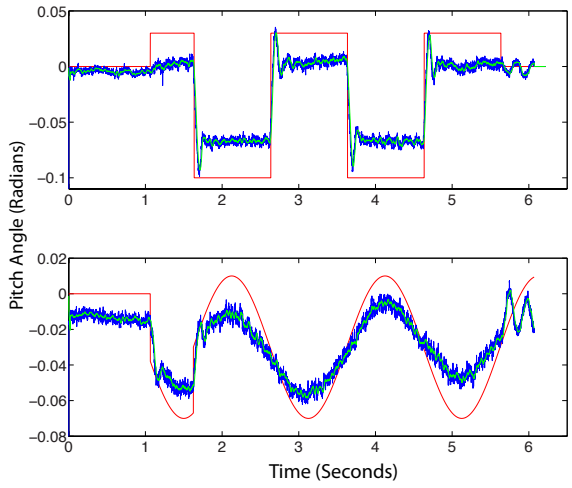

Fig. 7. Absolute angle control of the pitch axis of the RoboBee. The desired angle (red) is plotted alongside the raw magnetometer signal (blue) and the filtered magnetometer signal used by the controller (green).

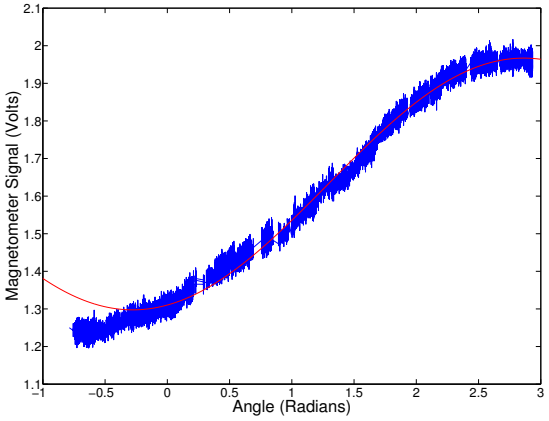

Fig. 8. Example calibration plot from the magnetometer. The measured angle in radians is along the x-axis and voltage signal from the sensor is along the y-axis. The raw signal from the magnetometer (blue) and the fitted curve (red) is plotted against the measured angle from Vicon in radians. Horizontal gaps are due to imperfect tracking by motion capture cameras. The divergence of the sinusoidal fit near -0.5 radians may be due to greater proximity of the magnets at that orientation on the wire.

θ_d is the desired pitch angle, and K_D is the derivative gain. The gains were then hand-tuned for this application.

As seen in Fig. 7, the magnetometer can provide sufficient orientation information to control the pitch angle of the bee, accurately tracking sinusoidal and square-wave trajectories. The first thing to note is that the desired orientations are not centered about zero. The RoboBee was unable to generate sufficient positive pitch torques and could only achieve a positive tilt angle of 0.03 radians. While maximum negative pitch torque could tilt the robot to a larger extent, the maximum angle that it could reach was -0.10 radians. The robot is unable to track the extreme values of the trajectory, which we can partially account for with the absence of an integral gain in the PID controller. With zero net torque applied to a flapping RoboBee, the angular estimate of the robot was slightly negative, demonstrated in the first second of the top and bottom figures of Fig. 7. The oscillation in the final half-second is due to the natural dynamics of the robot around the constraining wire. Using the existing experimental setup from [6], the magnetometer demonstrated sufficient bandwidth for absolute angle tracking. Furthermore, only one sensing axis was sufficient to measure the tilt angle.

IV. Yaw Control

Having demonstrated that the sensor can provide low latency orientation information for a FWMAV, we turned to using the sensor to control a degree of freedom that has not previously been controlled: yaw (heading) angle (Fig. 6). Torque measurements suggest the dual-actuator RoboBee design can induce yaw torques [22]. In [1], the RoboBee used a controller to damp the yaw rate, slowing the dynamics but did not control absolute heading of the vehicle.

During the pitch experiments, we measured the z-component of the magnetic field to have an angle of approximately 10° away from vertical, with an almost immeasurably

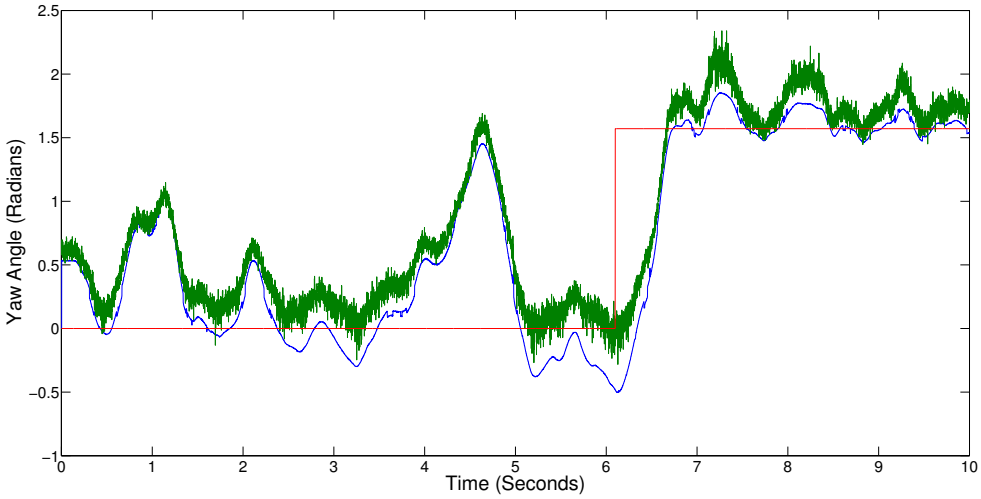

Fig. 9. Absolute Angle control of the yaw axis of the RoboBee. The desired angle (red) is plotted alongside the raw magnetometer signal (green), and the Vicon signal (blue).

small component in the x-y plane. As the direction of the magnetic field is aligned with the axis of rotation during these yaw experiments, the signal through 120° varied by only 0.1V, too low for control about the yaw axis. We therefore created a magnetic field with neodymium magnets (K&J Magnetics, Inc., Pipersville, PA USA) grade N42 with a surface magnetic field of 5,248Ga [23]. Separated by a distance of 12 cm the magnetic field strength at the magnetometer is theoretically 247mGa, with an in-plane field strength of 165 mGa – well within the sensitivity range of the sensor (Table I). The magnets were also oriented at an angle of approximately 45° from vertical to ensure a sufficient resolution as the sensor is rotated about yaw.

A. Calibration

We mounted the sensor to the anterior of the robot and attached the robot to a vertical wire that allowed vertical flight and rotation about the yaw axis, but prevented lateral flight and rotation about the pitch and roll axes (Fig. 1). Signals from the magnetometer were taken simultaneously with orientation information from Vicon that tracked reflective markers mounted to the robot as it rotated around the wire. The magnetometer signal and orientation information are plotted in Fig. 8. The signal was fitted with the three calibration parameters from equation (2); an example fit can be seen in red plotted over the raw magnetometer data in Fig. 8. Through 180°, the voltage signal had a range of approximately 800mV, with a measured standard deviation of 12mV; the resolution for these experiments is lower with an accuracy of 10° (0.17 radians). Given the controller and gain in [2], this uncertainty would cause the error in lateral position of around ±4cm in hovering flights because of the inability to distinguish between pitch and roll directions. Because of the position of the magnets, the sensor signal is monotonic between -30° and 150°, so we chose trajectories that fell in that range. We found that the robot had an equilibrium point on the wire around 45°, due to a slight inclination in the vertical guide wire and the presence of the tether.

B. Absolute Angle Control

The piezoelectric actuators were driven with a fixed voltage amplitude of 80V and a flapping frequency of 120Hz. Yaw torques are generated with split-cycle flapping, leading to asymmetric velocities that result in asymmetric drag forces on the wings [21] [22]. Electrically, the sinusoidal signal varies the rise time of one wing and varies the fall time of the other wing by adjusting the fraction of the second harmonic in the signal while maintaining peak to peak amplitude. How much this rise and fall time differ bilaterally determines the amount of torque applied to the body. The magnetometer signal was integrated into a feedback loop with a PD controller to adjust the fraction of second harmonic in the signal driving each wing. Using the PD control law (3) with measured and desired yaw angles to command yaw torque, we hand-tuned the gains for this specific experiment. Due to the larger noise range measured during heading calibration, the gain of the derivative term could not be increased, making the system underdamped.

Fig. 9 shows the results of a trial in which the magnetometer served as a sensor in a feedback loop to control yaw. The magnetometer can track the motion capture estimate, with a mean error of 0.10 radians. The maximum error between motion capture and sensor estimates was about 0.35 radians between five and six seconds. However, the robot is outside the calibration range during this time period and the calibration indicates an orientation of 0°. Though the vehicle tracks the general trend of the reference, and recovers from large errors, its performance is low, taking nearly a second to perform course changes. These results indicate that while the sensor can sufficiently estimate the true heading angle, further work may be necessary to find

drive signals that maximize yaw torque or to explore alternate designs [24]. Effects that lead to large errors between four and five seconds could be the result of external air currents, or due to the effect of downward flow produced by the wings, known as "downwash," causing instability. We also saw that the tether had a large effect on the orientation of the robot, changing its position slightly could greatly effect the orientation of the robot. Nevertheless, these results represent the first demonstration of heading control on a RoboBee.

V. Conclusions and Future Work

The magnetometer demonstrated low latency orientation information for an active feedback loop for absolute angle control around both the pitch and yaw axes. These results thus represent a step away from controlled flight using external power and Vicon toward onboard power and control systems. Onboard sensing is a critical step in achieving a fully autonomous robot. The sensor's low mass, small footprint, moderate power consumption, and high bandwidth make it a viable candidate for integration on future generations of the RoboBee.

For this work, the circuitry required to amplify this signal was not onboard the RoboBee and was not included in the mass and power budget. Increasing the number of axes can increase the amount of information about the orientation of the robot. The circuitry required would also increase for additional axes, as each axis requires a two-wire connection and two amplification stages. However, this could be achieved using one high gain amplifier and an analog multiplexer on an application-specific IC.

It has been shown that rotation rate is sufficient information to achieve upright stability on the RoboBee [25] [26]. Taking the derivative of the magnetometer signal may provide low-latency feedback because changes in magnetic field due to disturbances or translational motion will likely be slower than the rotation rate of the RoboBee. Rotational information from the magnetometer may prove to be less susceptible to noise from the vibration induced by flapping wings than a similarly sized gyroscope. The ocelli have proven capable of providing rotation rates for upright stability [26], and gyroscopes or a magnetometer may complement this signal. We will also explore the use of a magnetometer to determine heading angle in free flight, complementing the absolute position information from the optic flow sensors. In this scenario, the final sensor for feedback control on a fully autonomous RoboBee will include a number of low-level control sensors such as the ocelli and gyroscope for proprioception, as well as a magnetometer and optic flow sensor to determine absolute position and orientation.

Acknowledgements

The authors would like to thank Kevin Ma and Benjamin Finio for designing and fabricating the two generations of RoboBees used in this work. We would also like to acknowledge Kevin Galloway for fabricating the apparatus to tension and hold the wire used for the yaw control experiments, and Pakpong Chirarattananon for his assistance with estimating the error bounds on a hovering RoboBee. This work was partially supported by the National Science Foundation (award numbers CCF-0926148 and CMMI-0746638) and the Wyss Institute for Biologically Inspired Engineering. This material is based upon work supported by the National Science Foundation Graduate Research Fellowship under Grant No. (DGE1144152). Any opinions, findings, and conclusions or recommendations expressed in this material are those of the authors and do not necessarily reflect the views of the National Science Foundation.

References

[1] Ma, Kevin Y., Pakpong Chirarattananon, Sawyer B. Fuller, and Robert J. Wood. "Controlled Flight of a Biologically Inspired, Insect-Scale Robot." Science 340, no. 6132 (2013): 603-607.

[2] Chirarattananon, Pakpong, Kevin Y. Ma, Robert J. Wood. "Adaptive control for takeoff, hovering, and landing of a robotic fly." To appear in Intelligent Robots and Systems (IROS), 2013 IEEE/RSJ International Conference on. IEEE, 2013.

[3] Wu, Wei-Chung, Luca Schenato, Robert J. Wood, and Ronald S. Fearing. "Biomimetic sensor suite for flight control of a micromechanical flying insect: design and experimental results." In Robotics and Automation, 2003. Proceedings. ICRA, 2003. IEEE International Conference on, vol. 1, pp. 1146-1151. IEEE, 2003.

[4] Wu, Wei Chung, Robert J. Wood, and Ronald S. Fearing. "Halteres for the micromechanical flying insect." In Robotics and Automation, 2002. Proceedings. ICRA, 2002. IEEE International Conference on, vol. 1, pp. 60-65. IEEE, 2002.

[5] Duhamel, P-EJ, Nestor Osvaldo Perez-Arancibia, Geoffrey L. Barrows, and Robert J. Wood. "Altitude feedback control of a flapping-wing microrobot using an on-board biologically inspired optical flow sensor." In Robotics and Automation (ICRA), 2012 IEEE International Conference on, pp. 4228-4235. IEEE, 2012.

[6] Fuller, Sawyer B, Alexander Sands, Andreas Haggerty, Michael Karpelson, and Robert J. Wood. "Estimating attitude and wind velocity using biomimetic sensors on a microrobotic bee." In Robotics and Automation (ICRA), 2013 IEEE International Conference on, IEEE, 2013.

[7] Wajnberg, Eliane, Daniel Acosta-Avalos, Odivaldo Cambraia Alves, Jandira Ferreira de Oliveira, Robert B. Srygley, and Darci MS Esquivel. "Magnetoreception in eusocial insects: an update." Journal of the Royal Society Interface 7, no. Suppl 2 (2010): S207-S225.

[8] Wehner, Rudiger. "Neurobiology of polarization vision." Trends in neurosciences 12, no. 9 (1989): 353-359.

[9] Thomson, William. "On the Electro-Dynamic Qualities of Metals:–Effects of Magnetization on the Electric Conductivity of Nickel and of Iron." Proceedings of the Royal Society of London 8 (1856): 546-550.

[10] Baibich, Mario Norberto, J. M. Broto, Albert Fert, F. Nguyen Van Dau, F. Petroff, P. Etienne, G. Creuzet, A. Friederich, and J. Chazelas. "Giant magnetoresistance of (001) Fe/(001) Cr magnetic superlattices." Physical Review Letters 61, no. 21 (1988): 2472.

[11] Binasch, Grunberg, Peter Grunberg, F. Saurenbach, and W. Zinn. "Enhanced magnetoresistance in layered magnetic structures with antiferromagnetic interlayer exchange." Physical review B 39 (1989): 4828-4830.

[12] Daughton, J. M. "GMR applications." Journal of Magnetism and Magnetic Materials 192, no. 2 (1999): 334-342.

[13] McGuire, T., and R. Potter. "Anisotropic magnetoresistance in ferromagnetic 3d alloys." Magnetics, IEEE Transactions on 11, no. 4 (1975): 1018-1038.

[14] Tsang, Ching, Robert E. Fontana, Tsann Lin, David E. Heim, Virgil S. Speriosu, Bruce A. Gurney, and Mason L. Williams. "Design, fabrication and testing of spin-valve read heads for high density recording." Magnetics, IEEE Transactions on 30, no. 6 (1994): 3801-3806.

[15] Giebeler, C., D. J. Adelerhof, A. E. T. Kuiper, J. B. A. Van Zon, D. OelgeschlŁger, and G. Schulz. "Robust GMR sensors for angle detection and rotation speed sensing." Sensors and Actuators A: Physical 91, no. 1 (2001): 16-20.

[16] Reig, Candid, Mara-Dolores Cubells-Beltrn, and Diego Ramrez Muoz. “Magnetic field sensors based on giant magnetoresistance (GMR) technology: applications in electrical current sensing.” Sensors 9, no. 10 (2009): 7919-7942.

[17] Karpelson, Michael, Gu-Yeon Wei, and Robert J. Wood. “Driving high voltage piezoelectric actuators in microrobotic applications.” Sensors and Actuators A: Physical 176 (2012): 78-89.

[18] Caruso, Michael J., Tamara Bratland, Carl H. Smith, and Robert Schneider. “A new perspective on magnetic field sensing.” Sensors-Peterborough- 15 (1998): 34-47.

[19] Honeywell, “Three Axis Magnetic Sensor HMC1043, Revision G. Datasheet, August 2012.

[20] Karpelson, Michael, John Peter Whitney, Gu-Yeon Wei, and Robert J. Wood. “Energetics of flapping-wing robotic insects: Towards autonomous hovering flight.” In Intelligent Robots and Systems (IROS), 2010 IEEE/RSJ International Conference on, pp. 1630-1637. IEEE, 2010.

[21] Finio, Benjamin M., and Robert J. Wood. “Open-loop roll, pitch and yaw torques for a robotic bee.” Intelligent Robots and Systems (IROS), 2012 IEEE/RSJ International Conference on. IEEE, 2012.

[22] Ma, Kevin Y., Samuel M. Felton, and Robert J. Wood. “Design, fabrication, and modeling of the split actuator microrobotic bee.” In Intelligent Robots and Systems (IROS), 2012 IEEE/RSJ International Conference on, pp. 1133-1140. IEEE, 2012.

[23] K & J Magnetics - Strong Neodymium Magnets, Rare Earth Magnets. “K & J Magnetics – Products B633.” Web. 1 Sept. 2013.⟨http://www.kjmagnetics.com/proddetail.asp?prod=B633⟩.

[24] Teoh, Z. E., and Robert J. Wood. “A Flapping-Wing Microrobot with a Differential Angle-of-Attack Mechanism.” In Robotics and Automation (ICRA), 2013 IEEE International Conference on, IEEE, 2013.

[25] Teoh, Zhi Ern, Sawyer B. Fuller, Pakpong Chirarattananon, N. O. Perez-Arancibia, Jack D. Greenberg, and Robert J. Wood. “A hovering flapping-wing microrobot with altitude control and passive upright stability.” In Intelligent Robots and Systems (IROS), 2012 IEEE/RSJ International Conference on, pp. 3209-3216. IEEE, 2012.

[26] Fuller, Sawyer B., Michael Karpelson, Andrea Censi, Kevin Ma, and Robert J. Wood. “First Autonomous Flight of a Robotic Fly using Onboard Vision Sensors.” In preparation, 2013.